



1 **Effects of grain size and seawater salinity on magnesium hydroxide**
2 **dissolution and secondary calcium carbonate precipitation kinetics:**
3 **implications for ocean alkalinity enhancement**

4

5 Charly A. Moras^{1*}, Tyler Cyronak², Lennart T. Bach³, Renaud Joannes-Boyau¹ and Kai G. Schulz¹

6

7 ¹Faculty of Science and Engineering, Southern Cross University, Lismore, NSW, Australia

8 ²Institute for Coastal Plain Science, Georgia Southern University, Savannah, GA, USA

9 ³Ecology & Biodiversity, Institute for Marine and Antarctic Studies, University of Tasmania, Hobart, TAS, Australia

10

11 *Correspondence:* Charly A. Moras (c.moras.10@student.scu.edu.au)

12



13 **Abstract.** Understanding the impact that mineral grain size and seawater salinity have on magnesium hydroxide ($\text{Mg}(\text{OH})_2$)
14 dissolution and secondary calcium carbonate (CaCO_3) precipitation is critical for the success of ocean alkalinity enhancement.
15 We tested the $\text{Mg}(\text{OH})_2$ dissolution kinetics in seawater using three $\text{Mg}(\text{OH})_2$ grain sizes (<63 , $63\text{-}180$ and >180 μm) and at
16 three salinities (~ 36 , ~ 28 and ~ 20). While $\text{Mg}(\text{OH})_2$ dissolution occurred quicker the smaller the grain size, salinity did not
17 significantly impact measured rates. Our results also demonstrate that grain size can impact secondary CaCO_3 precipitation,
18 suggesting that an optimum grain size exists for ocean alkalinity enhancement (OAE) using solid $\text{Mg}(\text{OH})_2$. Of the three grain
19 sizes tested, the medium grain size ($63\text{-}180$ μm) was optimal in terms of delaying secondary CaCO_3 precipitation. We
20 hypothesize that in the lowest grain size experiments, the higher surface area provided numerous CaCO_3 precipitation nuclei,
21 while the slower dissolution of bigger grain size maintained a higher alkalinity/pH at the surface of particles, increasing CaCO_3
22 precipitation rates and making it observable much quicker than for the intermediate grain size. Salinity also played a role in
23 CaCO_3 precipitation where the decrease in magnesium (Mg) allowed for secondary precipitation to occur more quickly, similar
24 in effect size to another known inhibitor, i.e., dissolved organic carbon (DOC). In summary, our results suggest that OAE
25 efficiency as influenced by CaCO_3 precipitation not only depends on seawater composition but also on the physical properties
26 of the alkaline feedstock used.
27



28 1. Introduction

29 The concentration of carbon dioxide (CO₂) in the atmosphere has been in a relatively narrow band from ~180 to ~280
30 ppmv for the last 800,000 years, but has risen rapidly over the last 250 years to approximately 420 ppmv today (Lüthi et al.,
31 2008, Monnin et al., 2001, Siegenthaler et al., 2005). This is the result of increasing utilisation of fossil fuels, cement production
32 and land-use change, driving subsequent global climate change (IPCC, 2021). While about 42% of CO₂ emissions remain in
33 the atmosphere, and are mainly responsible for global warming, about 26% are currently absorbed by the oceans, leading to
34 ocean acidification (Friedlingstein et al., 2022, IPCC, 2021). To mitigate the effects of ocean acidification and slow down the
35 increase in Earth's global temperature, CO₂ reduction efforts are not sufficient and the use of carbon dioxide removal (CDR)
36 strategies have become necessary as a supplement to emission reduction (Hoegh-Guldberg et al., 2019).

37 One emerging marine CDR approach is ocean alkalinity enhancement (OAE). Over long timescales, the natural CO₂-
38 facilitated weathering of alkaline rocks supplies alkalinity to the oceans, influencing its CO₂ uptake potential and storage. OAE
39 builds upon this weathering feedback in the Earth System and can be accomplished by actively spreading pulverized alkaline
40 minerals in and around marine environments or electrochemically removing acidity from seawater (Eisaman et al., 2023). In
41 both cases, the seawater total alkalinity (TA) is increased thereby increasing the storage capacity of seawater for atmospheric
42 CO₂ (GESAMP, 2019, Kheshgi, 1995). On local scales around where the OAE perturbation is made, the increase in alkalinity
43 and pH may also mitigate ocean acidification (Hartmann et al., 2013).

44 Recent studies have investigated the carbonate chemistry changes following OAE, and a major outcome was the risk
45 for runaway calcium carbonate (CaCO₃) precipitation (Fuhr et al., 2022, Hartmann et al., 2023, Moras et al., 2022). There are
46 several inorganic CaCO₃ precipitation mechanisms that have been described in the literature (Morse et al., 2007, Pytkowicz,
47 1965). CaCO₃ can precipitate homogeneously in the absence of solid or soluble organic and inorganic particles, pseudo-
48 homogeneously in the presence of organic surfaces, and heterogeneously in the presence of mineral solids (Marion et al.,
49 2009). The key parameter that governs whether precipitation occurs is the calcium carbonate saturation state (Ω), which is
50 calculated from seawater Ca²⁺ and CO₃²⁻ concentrations as:

51

$$52 \quad \Omega = \frac{[Ca^{2+}][CO_3^{2-}]}{K_{sp}}$$

53

54 where [Ca²⁺] and [CO₃²⁻] are the concentrations of calcium and carbonate in solution, respectively, and K_{sp} the solubility
55 product of CaCO₃ in the solution. Ω is therefore closely related to the composition of the solution and its salinity, but is also
56 highly temperature dependent (Zeebe and Wolf-Gladrow, 2001). For aragonite, the CaCO₃ morphotype that inorganically



57 precipitates in modern seawater, the saturation state (Ω_A) has to be higher than 12.3 for pseudo-homogeneous precipitation to
58 occur in water with a salinity of 35 and at 25 °C (Marion et al., 2009). Homogeneous precipitation will occur at much higher
59 Ω_A values, while heterogeneous precipitation will occur already at much lower Ω_A but depends on the actual lattice
60 compatibility of CaCO_3 for the mineral particles present (Morse et al., 2007, Zhong and Mucci, 1989). Another important
61 aspect is that once precipitation becomes measurable, it will continue in a “runaway” fashion, i.e., quickly ramping up until it
62 slows down once Ω_A gets closer to 1 again.

63 Several studies have reported such behaviour upon mineral alkalinity addition (Fuhr et al., 2022, Hartmann et al.,
64 2023, Moras et al., 2022) with critical threshold of Ω_A of ~ 7.0 for the two calcium based OAE minerals of calcium oxide –
65 CaO – and calcium hydroxide – $\text{Ca}(\text{OH})_2$ – and report precipitation stopping at Ω_A values of 1.8-2.0 (Moras et al., 2022).
66 Precipitation has also been observed for magnesium-based minerals such as brucite or reagent grade magnesium hydroxide –
67 $\text{Mg}(\text{OH})_2$, but actual thresholds have not been determined (Hartmann et al., 2023). Furthermore, the effect of grain size,
68 determining factor of the surface area available for mineral dissolution and CaCO_3 precipitation, has not been studied.
69 Similarly, the effect of potential CaCO_3 precipitation inhibitors such as seawater magnesium (Mg) concentrations, governed
70 by salinity, and dissolved organic carbon (DOC), are relatively unknown (Chave and Suess, 1970, Millero et al., 2001, Pan et
71 al., 2021, Zhong and Mucci, 1989). This study focuses on the impact of $\text{Mg}(\text{OH})_2$ grain size on its dissolution kinetics in
72 natural seawater, as well as the impact of salinity. Furthermore, the subsequent runaway CaCO_3 precipitation that is triggered,
73 and its kinetics are reported. Finally, the effect of increased $[\text{Mg}]$ and $[\text{DOC}]$ in seawater on the CaCO_3 precipitation process
74 is explored.

75

76 2. Material and methods

77 2.1. Seawater collection and experimental setup

78 Seawater was collected in Broken Head, New South Wales, Australia (25°42'12" S, 153°37'03" E) using 25 L jerry
79 cans, about 200 m from the shore to avoid sampling sand and suspended particles. The collected seawater was stored in the
80 dark at 4 °C for three days to reduce microbial activity and allow particles to settle to the bottom, facilitating filtration. The
81 entire contents of the jerry cans were then sterile filtered using a peristaltic pump and a 0.2 μm Whatman Polycap 75 AS filter,
82 before being stored in cleaned and autoclaved 25 L polycarbonate bottles. Prior to conducting the experiments, each seawater
83 batch was equilibrated to laboratory air pCO_2 by bubbling them with H_2O -saturated air for at least a week (Moras et al., 2023).
84 This ensured comparable starting conditions for the various experiments. All experiments utilised reagent grade $\text{Mg}(\text{OH})_2$
85 (>98%, kindly supplied by Atlas Materials) which had been ground in a Pulverizer laboratory mill.



86

87 **2.2. Grain size and salinity experiments**

88 Approximately 1.5 litres of seawater were placed in a clean 2 L borosilicate 3.3 beaker, surrounded by a water jacket
89 set to 21 °C and controlled by a tank chiller line TK-1000. A floating lid with three ports was placed on the water surface,
90 allowing for concurrent Mg(OH)₂ addition, pH measurement and water sampling. Upon Mg(OH)₂ addition, the seawater was
91 incubated for 18 hours to allow for full Mg(OH)₂ dissolution. Thereafter the beaker content was transferred to a clean 1 L
92 borosilicate 3.3 Schott bottle which was tightly closed without any headspace to minimise CO₂ ingassing. The bottle was
93 placed on a stirring platform at 200 rpm in the dark, at room temperature (24.8 ± 1.3 °C). All grain size and salinity treatments
94 were run in triplicates for up to 34 days.

95 For the grain size experiments, three grain size ranges were produced using two stainless steel sieves with 63 µm and
96 180 µm mesh sizes. The medium range, i.e., 63-180 µm, was also used for the salinity experiments at ~36, ~28 and ~20. The
97 lower salinity seawater was produced by mixing natural seawater with MilliQ water. Exact salinities were determined on 200
98 mL of seawater sample equilibrated to room temperature in a gas tight polycarbonate container, by measuring conductivity
99 and temperature with a 914 pH/conductometer, and converted to salinity using the 1978 practical salinity scale (Lewis and
100 Perkin, 1981). For all experiments, Mg(OH)₂ additions were adjusted to yield an Ω_A of ~9 (Table 1) to allow for a significant
101 TA increase and secondary CaCO₃ precipitation, based on previously found thresholds for CaO and Ca(OH)₂ (Moras et al.,
102 2022).

103 In all the experiments, the first 18 hours of reaction were monitored by measuring the pH on the free scale (pH_F) with
104 an Aquatrode Plus with Pt1000 (Metrohm) connected to an 888 Titrande (Metrohm), before transferring the content of the 2
105 L beaker into the clean 1 L Schott bottles. A sample for TA and DIC measurements was taken before Mg(OH)₂ addition, and
106 after the 18 hours. The temperature and pH_F were then recorded twice a day until a sudden drop in pH_F was observed, linked
107 to CaCO₃ precipitation. A new sample for TA and DIC measurements was then taken. The time at which CaCO₃ runaway
108 precipitation was deemed to have started was considered to be the last stable pH_F measurement before the sudden drop. TA
109 and DIC samples were taken at varying intervals during CaCO₃ precipitation (see figures) to cover most of the CaCO₃
110 precipitation process, and at least 300 mL of water was reserved for two TA and DIC samples at the end of the experiment.
111 Between 9 and 10 TA and DIC samples per experiment were collected to monitor the changes in DIC and TA overtime. Their
112 decrease in a 2:1 ratio was further used to reconstruct TA and DIC from pH measurements in the experiments on the effect of
113 Mg and DOC on CaCO₃ precipitation (see below for details).

114



Table 1: Summary of the main experimental parameters for each of the incubations investigating the salinity and grain size effects on Mg(OH)₂ dissolution and CaCO₃ precipitation kinetics.

Experimental details	TA increase ($\mu\text{mol kg}^{-1}$)	Maximum Ω reached	Days of stable TA	Overall TA loss ($\mu\text{mol kg}^{-1}$)	Overall DIC loss ($\mu\text{mol kg}^{-1}$)	Final Ω
Salinity effect on Mg(OH)₂ dissolution and CaCO₃ precipitation kinetics						
<i>Salinity 36</i>						
Rep 1; Rep 2; Rep 3	555.5; 500.4; 534.9	9.23; 8.96; 9.16	10; 12; 9	1009.8; 1013.9; 1068.5	414.8; 477.4; 467.7	2.04; 1.95; 1.84
Mean \pm St. Dev.	530.3 \pm 27.8	9.12 \pm 0.14	10.33 \pm 1.53	1030.8 \pm 32.8	456.7 \pm 27.9	1.94 \pm 0.10
<i>Salinity 28</i>						
Rep 1; Rep 2; Rep 3	618.7; 660.9; 615.8	9.18; 9.48; 9.29	6; 6; 4	1060.9; 1104.8; 1096.8	487.0; 494; 529.5	1.74; 1.68; 1.63
Mean \pm St. Dev.	631.8 \pm 25.3	9.32 \pm 0.16	5.33 \pm 1.15	1087.5 \pm 23.4	503.5 \pm 22.8	1.68 \pm 0.05
<i>Salinity 20</i>						
Rep 1; Rep 2; Rep 3	575.9; 591.2; 605.3	8.26; 8.49; 9.14	2; 2; 1	899.3; 963.3; 1062.9	481.4; 522.8; 603.6	1.54; 1.51; 1.50
Mean \pm St. Dev.	590.8 \pm 14.7	8.63 \pm 0.45	1.67 \pm 0.58	975.2 \pm 82.4	535.9 \pm 62.1	1.52 \pm 0.02
Grain size effect on Mg(OH)₂ dissolution and CaCO₃ precipitation kinetics						
<i>Small Grain size</i>						
Rep 1; Rep 2; Rep 3	422.9; 447.5; 412.1	8.60; 8.48; 8.22	7; 4; 3	1019.3; 1021.9; 988.3	562.2; 547.3; 550.6	2.06; 2.16; 2.14
Mean \pm St. Dev.	427.5 \pm 18.1	8.43 \pm 0.20	4.67 \pm 2.08	1009.8 \pm 18.7	553.4 \pm 7.8	2.12 \pm 0.05
<i>Medium Grain size</i>						
Rep 1; Rep 2; Rep 3	555.5; 500.4; 534.9	9.23; 8.96; 9.16	10; 12; 9	1009.8; 1013.9; 1068.5	414.8; 477.4; 467.7	2.04; 1.95; 1.84
Mean \pm St. Dev.	530.3 \pm 27.8	9.12 \pm 0.14	10.33 \pm 1.53	1030.8 \pm 32.8	456.7 \pm 27.9	1.94 \pm 0.10
<i>Large Grain size</i>						
Rep 1; Rep 2; Rep 3	368.9; 272.3; 412.6	8.41; 7.92; 8.72	3; 3; 2	1032.8; 980.7; 1103.1	606.1; 661.4; 647.5	1.89; 1.90; 2.02
Mean \pm St. Dev.	351.3 \pm 71.8	8.35 \pm 0.40	2.67 \pm 0.58	1038.9 \pm 61.4	638.3 \pm 28.8	1.93 \pm 0.07



116 **2.3. Manipulation of dissolved inorganic carbon and magnesium**

117 The seawater dilution by MilliQ to decrease salinity also decreased the concentration of various seawater components,
118 such as Mg and DOC concentrations. To disentangle a potentially general effect of salinity on $\text{Mg}(\text{OH})_2$ dissolution and
119 secondary precipitation kinetics from reductions in Mg and DOC concentrations, two additional experiments were designed.
120 In the first, the experiments at a salinity of 20 were replicated, but the Mg concentration was increased to a concentration
121 representative for a salinity of 35, i.e., $52.8 \text{ mmol kg}^{-1}$ (Dickson et al., 2007), by magnesium chloride (MgCl_2) addition from
122 a 3 M stock solution (molarity verified by inductively coupled plasma mass spectrometer measurements). This experiment was
123 run in triplicate. For the second experiment, a DOC-enriched seawater solution at the salinity of 20 was produced by
124 ultrafiltration (molecular weight cut-off of 2,000 Daltons, Vivaflow200 Hydrosart, Sartorius). A DOC gradient was then
125 created in five bottles by mixing the DOC-enriched salinity 20 seawater with the MilliQ-diluted seawater. The DOC
126 concentrations ranged from approximately $120 \mu\text{mol kg}^{-1}$ to approximately $325 \mu\text{mol kg}^{-1}$.

127 In both the Mg and DOC experiments, dissolution and secondary CaCO_3 precipitation kinetics were mainly monitored
128 by pH_F measurements, although a sample for TA and DIC was also taken before $\text{Mg}(\text{OH})_2$ addition and at the end of each
129 treatment. These samples, coupled to the pH_F measurements, allowed the changes in TA and DIC to be estimated over time.
130 The reconstruction occurred in two steps, where the increase in pH following $\text{Mg}(\text{OH})_2$ was assumed to be linked to an increase
131 of TA at constant DIC. Then, any decrease in pH was assumed to be due to CaCO_3 precipitation, so the estimated TA and DIC
132 loss after $\text{Mg}(\text{OH})_2$ dissolution were decreasing in a 2:1 ratio, as observed in the salinity and grain size experiments. Finally,
133 to account for CO_2 ingassing over time, the difference between estimated maximum TA and final measured TA was used as a
134 proxy. Half of the difference, representing CaCO_3 precipitation, was used to estimate the theoretical DIC loss. Once compared
135 to the final measured DIC, an ingassing rate was estimated.

136

137 **2.4. Analytical procedures**

138 The pH electrode was calibrated using three Metrohm buffer solutions (pH 4, 7 and 9), corresponding to a pH
139 measurement on the free scale. TA analyses were conducted using a potentiometric titration with an 848 Titrino Plus, coupled
140 to an 869 Compact Sample Changer from Metrohm. A 0.05M HCl solution with the ionic strength adjusted to 0.72 mol kg^{-1}
141 (representative for a salinity of 35) using NaCl was used as the titrant (Dickson et al., 2007). The DIC concentration was
142 measured using an Automated Infra-Red Inorganic Carbon Analyzer (AIRICA) coupled to a LI-COR Li7000 Infra-Red
143 detector (Gafar and Schulz, 2018). Both TA and DIC measurements were corrected against in-house reference material
144 (previously calibrated against certified reference material), with measurement uncertainties of ± 2.20 and $\pm 1.98 \mu\text{mol kg}^{-1}$
145 (Moras et al., 2023). Ω_A and carbonate chemistry speciation were calculated from TA and DIC, providing temperature and
146 salinity measurements, using CO2SYS (Sharp et al., 2021).



147 For scanning electron microscopy (SEM), discrete samples of about 10 mL of TA enriched seawater were filtered
148 through 0.2 μm polycarbonate filters (Whatman Cyclopore). These filters were rinsed with 20 mL of MilliQ to remove salts
149 and dried overnight at 60 °C. Once dried, the filters were kept in a desiccator until analysis. The filters were attached to double-
150 sided carbon tabs and placed on aluminium mounts before being coated with gold. SEM analysis was performed using a
151 tabletop Scanning Electron Microscope TM4000 Plus from Hitachi, coupled to an Energy Dispersive X-Ray (EDX) Analyser,
152 allowing to determine the elemental composition of observed particles.

153 The concentration of the MgCl_2 stock solution was measured by inductively coupled plasma mass spectrometer (ICP-MS)
154 measurements using an Agilent 7700 ICP-MS, coupled to a laser ablation unit (NWR213, Electro Scientific Industries, Inc.).
155 Seawater reference materials from the National Research Council of Canada NASS-6 were used to correct the measurements.
156 The DOC concentration of the DOC-enriched stock solution was determined using a Thermo Fisher Flash Elemental Analyzer
157 after acidifying the sample with nitric acid (Carvalho, 2023).

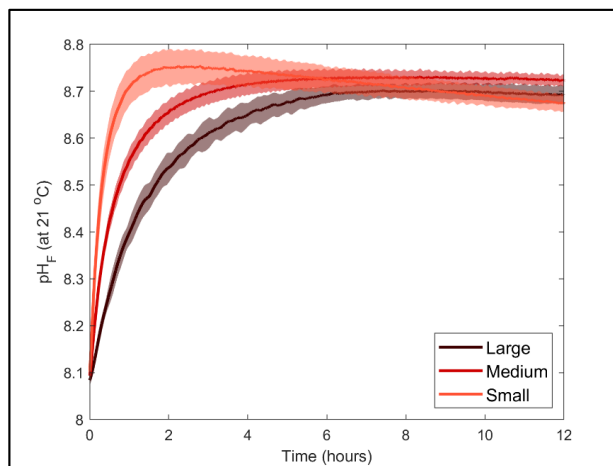
158

159 3. Results

160 3.1. Grain size effects on $\text{Mg}(\text{OH})_2$ dissolution kinetics

161 Three $\text{Mg}(\text{OH})_2$ grain sizes were dissolved in seawater at a salinity of ~ 36 (Figure 1). The starting pH_F was similar
162 for all incubations, with 8.11 ± 0.03 , 8.09 ± 0.01 and 8.07 ± 0.03 , for the small ($< 63 \mu\text{m}$), medium ($63\text{-}180 \mu\text{m}$) and large (> 180
163 μm) grain sizes, respectively. Upon dissolution, pH_F increased quite rapidly, reaching a maximum after about two hours for
164 the small particle size experiments, and about 6 to 8 hours in the medium and large particle size experiments (Figure 1). In
165 each incubation, a logarithmic trend in pH_F was observed, with the dissolution being much quicker for smaller grain sizes.
166 After two hours, the maximum pH_F recorded for the smaller grain size was 8.76 ± 0.04 , which continuously decreased to 8.68
167 ± 0.00 between 11 and 12 hours after $\text{Mg}(\text{OH})_2$ addition. In contrast, the pH_F for the medium and larger grain size increased to
168 8.72 ± 0.00 and 8.68 ± 0.03 after about eight hours and remained stable thereafter, respectively (Figure 1).

169



170

171 **Figure 1: Changes in pH_F at 21 °C following dissolution of three Mg(OH)₂ grain sizes in natural seawater over 12 hours. Each grain**
172 **size was run in triplicate, with the average presented as the solid lines and the standard deviation range as the transparent areas.**

173

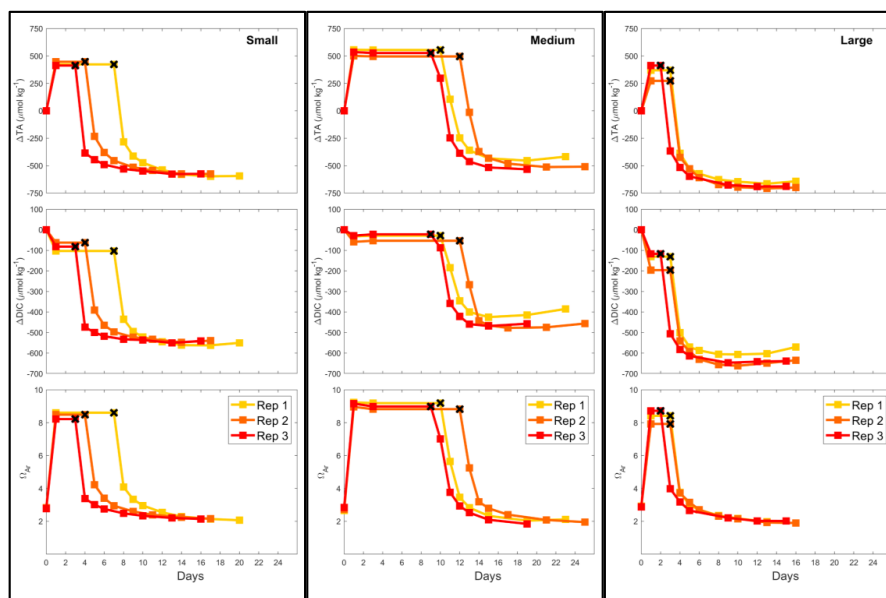
174 3.2. Grain size effect on CaCO₃ precipitation kinetics

175 The pH increase was reflected by increasing TA, measured prior to the Mg(OH)₂ addition and 18 hours later, by about
176 430, 530 and 350 μmol kg⁻¹, in the small, medium and large grain size incubations, respectively (Figure 2). The TA remained
177 stable for 3-7 days, 9-12 days, and 2-3 days before dropping in each grain size treatment (small, medium, large). In all
178 incubations, TA concentrations decreased in a similar fashion, with a strong drop the first two days, before slowly decreasing
179 for another week and stabilising. The overall TA loss for the duration of the experiments was ~1035 μmol kg⁻¹ in the medium
180 and large grain size incubations, while the TA dropped by about 1010 μmol kg⁻¹ in the small grain size incubations (Table 1).

181 The changes in Ω_A followed a similar pattern as TA, increasing from ~2.8 on average to ~9.1 in the medium grain
182 size incubation, and to ~8.4 in the small and large grain size experiments. Ω_A dropped at the same time as TA in the respective
183 experiments, stabilising around ~2.0 in all experiments.

184 Finally, a small drop in DIC was observed after Mg(OH)₂ addition in all experiments, of about 80, 30 and 140 μmol
185 kg⁻¹ in the small, medium and large grain size incubations, respectively. The DIC remained then relatively stable until the rapid
186 TA drop, where the overall DIC drops for the small, medium and large grain size incubations were calculated at ~550, ~455
187 and ~640 μmol kg⁻¹, respectively. While TA and Ω_A remained stable after this drop, DIC slightly increased, particularly
188 obvious in the medium and larger grain size incubations.

189



190

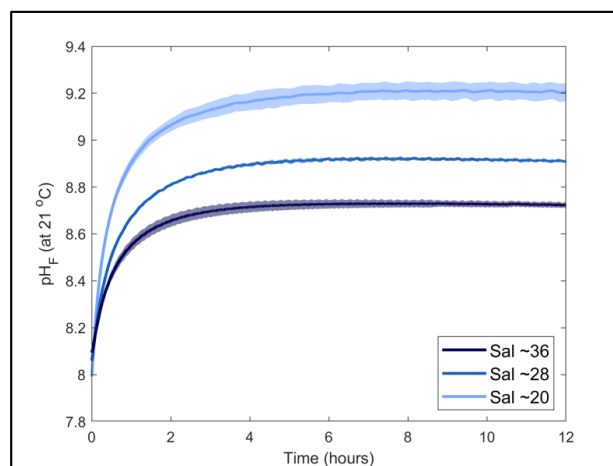
191 **Figure 2: Changes in TA, DIC and Ω_A during dissolution of three $Mg(OH)_2$ grain sizes in natural seawater over up to 25 days. Three**
 192 **replicates were conducted for each grain size and are represented in red, orange and yellow. The last stable TA and DIC conditions**
 193 **estimated by pH_F measurements are represented by a black cross.**

194

195 3.3. Salinity effect on $Mg(OH)_2$ dissolution kinetics

196 To test the salinity effect on $Mg(OH)_2$ dissolution and $CaCO_3$ precipitation kinetics, three sets of experiments were
 197 conducted in three different salinities, i.e., 20.38, 28.47 and 35.80, and using medium grain size $Mg(OH)_2$. From here on the
 198 salinities 20.38, 28.47 and 35.80 will be referred to as salinities 20, 28 and 36, respectively. Similarly to the grain size
 199 experiments, the dissolution of $Mg(OH)_2$ occurred rapidly in all three salinities, with the maximum pH_F being recorded after
 200 approximately 8 hours (Figure 3). Starting pH_F were slightly different, recorded at 7.99 ± 0.05 , 8.06 ± 0.01 and 8.09 ± 0.01 in
 201 the salinity 20, 28 and 36 incubations, and increased to a maximum of $9.19, \pm 0.00$, 8.91 ± 0.00 and 8.72 ± 0.00 , respectively.
 202 In all incubations, similar logarithmic trends were observed for pH_F (Figure 3).

203



204

205 **Figure 3: Changes in pH_F at 21 °C following $Mg(OH)_2$ dissolution in three different seawater salinities over 12 hours. Each salinity**
206 **has been run in triplicate, with the average presented as the solid lines and the standard deviation range as the transparent areas.**
207 **Please note that different maximum pH levels were reached because of increasing $Mg(OH)_2$ additions with decreasing salinity to**
208 **reach a similar Ω_A .**

209

210 3.4. Salinity effect on $CaCO_3$ precipitation kinetics

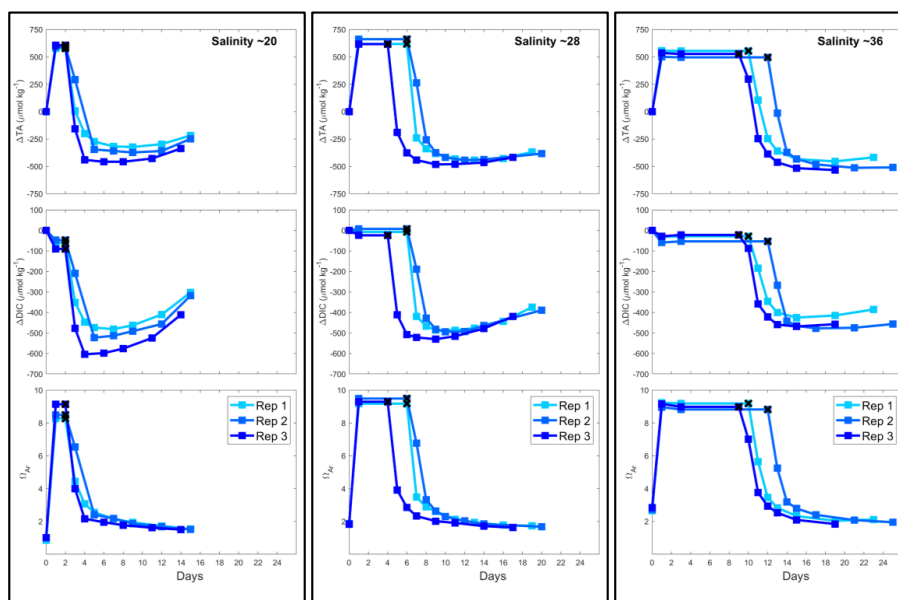
211 In all incubations, TA was increased as suggested by the pH_F trends, by ~ 590 , ~ 630 and $\sim 530 \mu\text{mol kg}^{-1}$ in the salinity
212 20, 28 and 36 incubations, respectively (Figure 4). The TA remained stable for different periods of time in each treatment; 1-
213 2 days in the salinity 20 incubations, 4-6 days in the salinity 28 incubations, and 9-12 days in the salinity 36 incubations.
214 Thereafter, TA dropped quickly the first two days in all incubations and stabilised quickly in the salinity 20 experiments. In
215 the salinity 28 incubations, the TA slowly decreased over five days after the first strong drop and stabilised, while in the salinity
216 36 experiments, the TA decreased slowly after the initial drop over seven days before stabilising. The overall TA losses for
217 salinities 20, 28 and 36 experiments were estimated at ~ 975 , ~ 1090 and $\sim 1030 \mu\text{mol kg}^{-1}$, respectively (Table 1).

218 Ω_A values followed a similar pattern as TA in all experiments. The starting Ω_A were different, varying between 1.0
219 for the salinity 20 incubations to 2.0 and 2.8 for the salinity 28 and 36 incubations, respectively. Similarly, following $Mg(OH)_2$
220 additions, Ω_A quickly increased to reach 8.6, 9.3 and 9.1 with increasing salinity. Together with TA, Ω_A eventually started
221 dropping, and then stabilised at different values, around 1.5 for a salinity of 20, around 1.7 for a salinity of 28 and around 2.0
222 for a salinity of 36.

223 Finally, DIC also decreased upon $Mg(OH)_2$ additions. An initial DIC drop was observed directly after $Mg(OH)_2$
224 additions of about $60 \mu\text{mol kg}^{-1}$ at the lowest salinity and $30 \mu\text{mol kg}^{-1}$ at the highest salinity. At a salinity of 28, a much
225 smaller DIC drop was observed in one replicate. After a period of stable DIC conditions, DIC also dropped in a similar fashion



226 as TA, with an overall DIC loss of about 535, 505 and 455 $\mu\text{mol kg}^{-1}$ from the lower to higher salinity incubations. While no
 227 DIC increase was observed towards the end of the experiment in the salinity 36 incubations, strong DIC increases were
 228 observed in the salinity 28 incubations and even more prominent ones in the salinity 20 incubations.
 229



230

231 **Figure 4: Changes in TA, DIC and Ω_A during $\text{Mg}(\text{OH})_2$ dissolution in three different salinities over up to 25 days. Three replicates**
 232 **were conducted for each salinity and are represented in shades of blue. The last stable TA and DIC conditions estimated by pH_f**
 233 **measurements are represented by a black cross.**

234

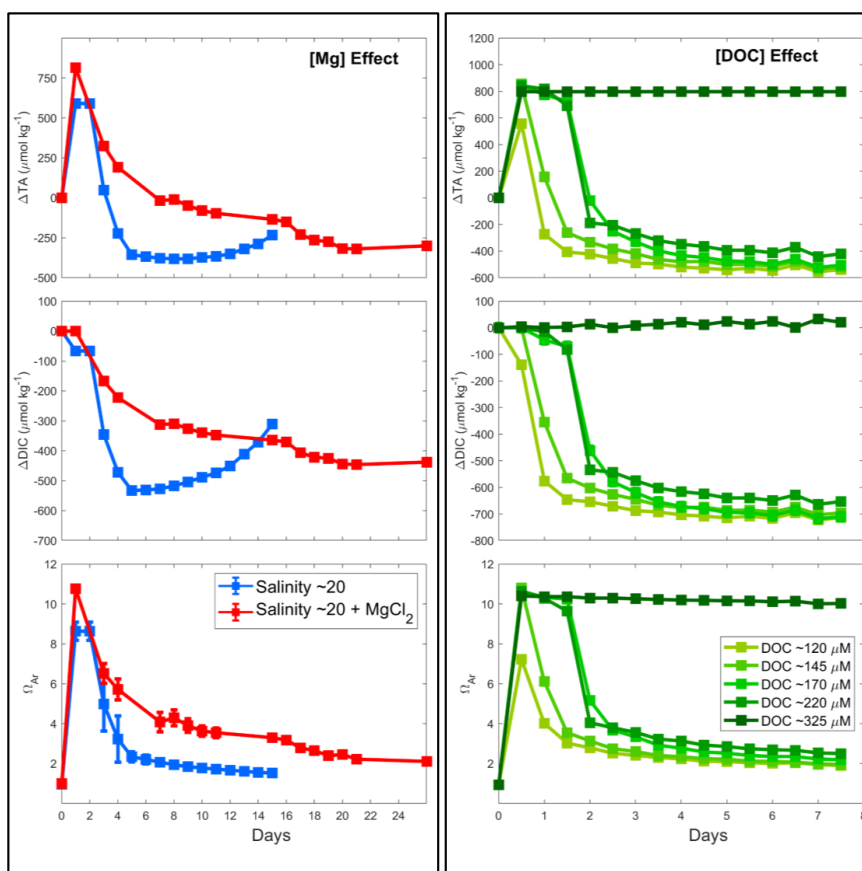
235 3.5. Magnesium and DOC effect on CaCO_3 precipitation

236 A similar pattern was observed for the salinity 20 experiments at natural and increased Mg concentrations, i.e., a rapid
 237 increase in TA reaching a maximum on day one, followed by a steady decline over the next two weeks (Figure 5). The
 238 maximum ΔTA reached was slightly different, with about 600 $\mu\text{mol kg}^{-1}$ of TA increase in the salinity 20, and nearly 800
 239 $\mu\text{mol kg}^{-1}$ in the salinity 20 + MgCl_2 incubations. Another interesting difference is the slower TA decrease with MgCl_2
 240 compared to the salinity 20. After about 18 days, the lowest ΔTA was reached while it only took about 6 days for the salinity
 241 20 ΔTA to reach the minimum. Similarly, DIC appeared to decrease less rapidly when MgCl_2 was present and Ω_A followed a
 242 similar trend after the initial strong increase.

243 Out of the five DOC experiments, four incubations showed a drop in TA (Figure 5). Similar maximum ΔTA were
 244 reached in most experiments, with a ΔTA of $\sim 800 \mu\text{mol kg}^{-1}$. However, in the incubation with $\sim 120 \mu\text{mol kg}^{-1}$, the TA increased



245 only by $\sim 600 \mu\text{mol kg}^{-1}$. Following this increase, TA decreased within a day in both 120 and 145 $\mu\text{mol kg}^{-1}$ DOC incubations,
 246 and stayed stable until day 3 in incubations with 170 and 220 $\mu\text{mol kg}^{-1}$. These four incubations also show a similar levelling
 247 pattern over time, even though it appears that in the higher DOC incubations, the total loss in TA was lower than for the lower
 248 DOC incubations. ΔDIC also follow a similar trend to ΔTA , with an early drop at 120 $\mu\text{mol kg}^{-1}$ of DOC, a drop after one day
 249 at 145 $\mu\text{mol kg}^{-1}$ of DOC, and a slow decrease from day 1 and a stronger drop on day 2 at 170 and 220 $\mu\text{mol kg}^{-1}$ of DOC. Ω_A
 250 followed a very similar pattern to ΔTA , with final Ω_A being higher in the experiments with higher DOC concentrations. Finally,
 251 in the experiment with the highest DOC concentration, i.e., 325 $\mu\text{mol kg}^{-1}$, no drop in TA, DIC or Ω_A was observed (the
 252 experiment was run for 42 days).
 253



254
 255 **Figure 5: Comparison of the reconstructed TA, DIC and Ω_A changes at 21 °C following $\text{Mg}(\text{OH})_2$ addition in seawater with salinity**
 256 **of 20 (blue), and in seawater with salinity 20 and Mg concentration equal to a salinity 35 (red), and in seawater with varying DOC**
 257 **concentrations (green).**

258



259 **4. Discussion**

260 **4.1. Grain size and salinity effects on Mg(OH)₂ dissolution**

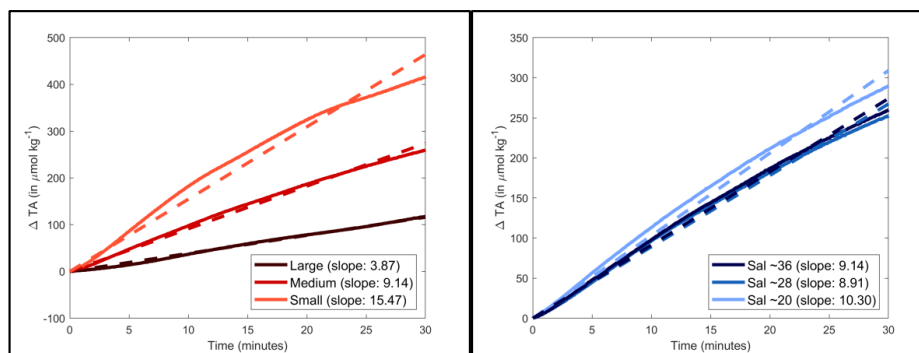
261 Maximum Mg(OH)₂ dissolution directly after its addition was negatively correlated with grain size (Figure 1, Figure
262 3). The smaller the grain size, the faster the maximum pH_F is reached, indicative of complete dissolution. This can be explained
263 by the fact that smaller particles have a larger surface area per gram of material than larger ones. The increasing dissolution
264 rate with decreasing particle size is particularly noticeable in when TA changes were estimated by using the pH_F data and
265 starting DIC measurements (Figure 6). Assuming a constant DIC over the first 30 minutes of reaction, i.e., no significant
266 CaCO₃ precipitation and/or CO₂ ingassing, TA can be reconstructed using CO2SYS. The maximum ΔTA reached with the
267 larger particle size occurred within 8 hours while it only took about 2 hours for the ΔTA to reach a maximum with small
268 particle size. The initial dissolution rate, i.e., within the first 30 minutes, was also significantly different between the various
269 grain sizes. The TA generation of smaller grain size particles was estimated at about 796.5 ± 7.1 μmol of TA mg⁻¹ min⁻¹. The
270 medium particles dissolved about twice as slow over the first 30 minutes, estimated at 391.6 ± 2.6 μmol of TA mg⁻¹ min⁻¹,
271 while the larger grain sizes dissolved more than four times slower, with about 168.7 ± 6.9 μmol of TA mg⁻¹ min⁻¹. Another
272 important difference between the smaller grain size experiments and the two others is the constant decrease in pH_F observed
273 right after reaching the maximum pH_F value. This decrease in pH_F can only be linked to either CaCO₃ precipitation, decreasing
274 TA and ultimately pH_F, or CO₂ ingassing, increasing the dissolved CO₂ concentration and ultimately decreasing the pH_F. The
275 constant and linear trend suggest that the latter is responsible for the decrease. If CaCO₃ was responsible for these pH_F changes,
276 the changes would follow a similar pattern to a negative exponential function. This is due to the fact that the more CaCO₃
277 nucleate, the more surface becomes available for further nucleation (Zhong and Mucci, 1989). However, in our case, the
278 changes appear linear. Such a pattern is indicative of CO₂ ingassing at an early stage, i.e., before the ingassing starts plateauing,
279 dictated by the difference between atmospheric and seawater pCO₂. Such ingassing is also occurring in the other experiments,
280 but is likely hidden by the stronger pH_F increase occurring during Mg(OH)₂ dissolution.

281 For salinity, we did not observe major differences in initial dissolution rates within the range of salinities tested, with
282 dissolution rates for salinities 36, 28 and 20 estimated at 391.6 ± 2.6, 359.8 ± 0.2 and 301.9 ± 0.3 μmol of TA mg⁻¹ min⁻¹,
283 respectively. Overall, TA generation potential of smaller grain size Mg(OH)₂ (<63 μm) at a salinity 36 was similar to that of
284 Ca(OH)₂ (Moras et al., 2022) which was also sieved through 63 μm. Assuming the same molar TA generation potential, the
285 same maximum Ω_A should have been reached. However, for Ca(OH)₂ it was ~7.4, while our small grain size Mg(OH)₂
286 incubations reached a maximum Ω_A of ~8.4. Such a difference is likely due to the difference in the starting conditions. In the
287 experiments shown here, the starting Ω_A was ~2.8 while it was about ~2.5 in Moras et al. (2022). This is explained by the
288 difference in the starting water composition and salinity, ultimately affecting the final Ω_A despite similar TA increases.
289 However, dissolution kinetics appear to differ between the minerals, with Ca(OH)₂ dissolving within 20-30 minutes while it
290 took two hours for Mg(OH)₂. These two minerals still dissolve at a relatively quick pace compared to other OAE feedstocks,



291 for instance olivine (Montserrat et al. 2017). Olivine took much longer to dissolve, with a maximum increase in pH recorded
 292 of ~0.15 units within 4-9 days. Ca(OH)₂ and Mg(OH)₂ additions required ~20 mg of materials, while to obtain such olivine
 293 results, more than 30 g of olivine were added per kg of filtered seawater, meaning that the TA generation potential is several
 294 orders of magnitude lower.

295



296

297 **Figure 6: Normalised changes in TA over the first 30 minutes following Mg(OH)₂ additions of three different grain sizes in natural**
 298 **seawater (left) and in three different salinities (right). A linear fit was calculated and is represented by the dashed line, and each**
 299 **slope is reported in the legend in between parentheses.**

300

301 4.2. Grain size and salinity effect on CaCO₃ precipitation

302 In all experiments, Mg(OH)₂ additions had been chosen to reach an Ω_A at which secondary CaCO₃ precipitation would
 303 be expected based on our experience with CaO and Ca(OH)₂ (Moras et al., 2022). Based on our suspicion that CaCO₃ might
 304 precipitate on magnesium-rich particles less easily than onto calcium-rich particles we chose a saturation state of ~9, slightly
 305 higher than the level of ~7 observed for CaO and Ca(OH)₂ (Moras et al., 2022). Precipitation kinetics were similar for all grain
 306 sizes, i.e., after the first precipitation was observed a new steady state was achieved in about two weeks. Precipitation
 307 seemingly stopped at Ω_A values close to 2.0 in experiments with seawater at a salinity of 36, similar to observations made by
 308 Moras et al. (2022) using CaO and Ca(OH)₂. For the smallest grain size, TA was stable for 3-7 days, which is longer than what
 309 has been observed for CaO and Ca(OH)₂ at the same size (Moras et al., 2022). This could be related to higher lattice
 310 compatibility of CaCO₃ for calcium-based minerals when it comes to precipitation onto mineral surfaces (Lioliou et al., 2007).
 311 Interestingly, however, the rate at which CaCO₃ precipitated was similar for CaO and Mg(OH)₂, while Ca(OH)₂ took almost
 312 twice as long to reach a new steady state (compare Figure 1 with Figure 2 in Moras et al., 2022).

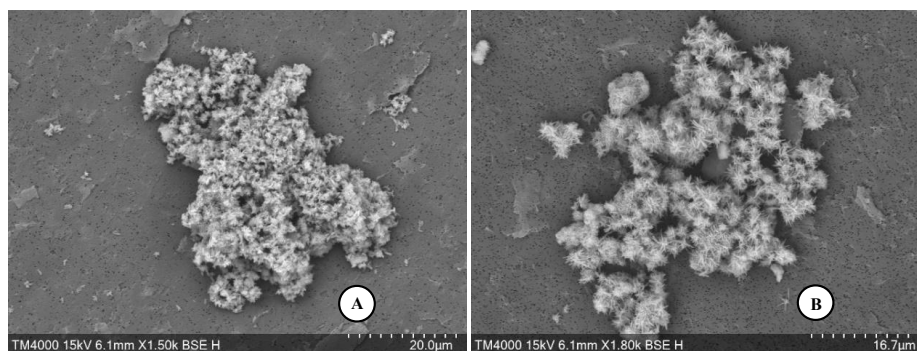
313 TA remained stable for longer, i.e., 9-12 days with medium grain size. However, similarly to the smaller grain size
 314 experiments, the TA was also less stable with the larger grain size, i.e., 2-3 days. As such, there appears to be an optimum



315 grain size for keeping TA stable for longer. To explain this, there must be two opposing processes at work. As discussed
316 earlier, smaller particles have larger surface area per gram of material than larger ones, i.e., smaller particles in our experiments
317 had on average more than 23 times the area of larger particles for the same amount of material, assuming round particles of 63
318 and 180 μm , respectively. Hence, heterogeneous precipitation will be quicker for smaller particles (Zhong and Mucci, 1989).
319 In contrast, what could favour quicker precipitation for larger particles with smaller surface area remains to be understood.
320 Here, it could be higher pH levels and hence Ω_A that are reached at a particle's surface as of having a larger diffusive boundary
321 layer. Hence, pH and Ω_A levels are likely to be much higher and remain for longer due to the slower dissolution of larger
322 particles at the site of CaCO_3 nucleation, which positively affects CaCO_3 precipitation rates.

323 To our surprise, EDX analysis did not reveal significant magnesium concentrations in early precipitated aragonite
324 crystals, i.e., ~18 hours after $\text{Mg}(\text{OH})_2$ addition. The presence of Mg could have been expected if CaCO_3 precipitated
325 heterogeneously onto $\text{Mg}(\text{OH})_2$ particles (Figure 7). The absence of Mg after EDX analysis suggests that while some $\text{Mg}(\text{OH})_2$
326 could have been used as a precipitation nuclei for CaCO_3 early on, it completely dissolved within the first 18 hours. Only the
327 freshly precipitation CaCO_3 would then remain in suspension, eventually acting as precipitation nuclei for runaway CaCO_3
328 precipitation. Finally, it is interesting to highlight that some traces of early aragonite crystals were present in all experiments,
329 and that the needle-shaped crystals were two to three times smaller in the larger grain size experiments than those sampled at
330 the end of the medium grain size experiments (Figure 7). One explanation that supports the previously mentioned boundary
331 layer theory is that the larger grain size particles, dissolving at a slower pace, maintained a Mg-rich environment while CaCO_3
332 started nucleating. The presence of this Mg during nucleation could have ultimately prevented CaCO_3 to fully form as bigger
333 needle-like crystals. However, these are speculations that are hard to prove or disprove.

334



335

336 **Figure 7: SEM images of aragonite crystals, sampled ~18 hours after larger $\text{Mg}(\text{OH})_2$ grain size addition (A) and sampled at the end**
337 **of the medium grain size incubations (B).**

338



339 **4.3. The role of dilution and potential effects of Mg and DOC concentrations**

340 The role of Mg in inhibiting CaCO₃ nucleation is well known (Morse et al., 2007, Pan et al., 2021, Pytkowicz, 1965).
341 Another known CaCO₃ nucleation inhibitor is organic matter, particularly dissolved organic matter (Chave and Suess, 1970).
342 While the role of organic matter is not as well understood as Mg, both have been linked to a decrease in CaCO₃ nucleation and
343 precipitation rates.

344 In our experiments involving dilution with MilliQ water, all dissolved components of the seawater were diluted,
345 including Mg and DOC. Such decreases could explain the quicker CaCO₃ precipitation in the salinity 20 experiments compared
346 to salinity 36, as lower Mg and DOC concentrations were not inhibiting precipitation as in the higher salinity treatments. To
347 test this, a new salinity 20 batch was prepared in triplicate and Mg was added to raise the total Mg concentration to ~52 mmol
348 kg⁻¹, similar to the Mg concentration in natural seawater at a salinity 35. The Mg increase did affect CaCO₃ precipitation
349 kinetics as shown by changes in TA (Figure 5), being slightly slower and apparently reaching a new steady state at higher ΔTA
350 and Ω_A. Furthermore, it is important to highlight that despite CaCO₃ precipitation being triggered at a similar time, i.e., within
351 1 to 2 days, a difference was observed regarding the maximum ΔTA reached. In the salinity 20 + MgCl₂ experiments, the
352 maximum ΔTA value was higher than the one in the salinity 20 experiments. This suggests that with a higher dissolved Mg
353 concentration, less CaCO₃ is precipitated early on. Following this early precipitation, an overall slower precipitation rate is
354 observed until reaching a steady state (Figure 5).

355 However, the slightly reduced CaCO₃ precipitation rate due to decreased Mg concentrations alone cannot explain
356 such stark differences in TA stability between the salinity 36 and 20 experiments (Figure 4). It is most likely linked to both
357 the decrease in Mg and DOC concentrations when diluting with MilliQ. The gradient of five salinity 20 replicates with
358 increasing DOC concentrations clearly showed that secondary CaCO₃ precipitation could be delayed by modifying the DOC
359 concentrations alone. For instance, secondary precipitation became already measurable after 12 hours at DOC concentrations
360 of 120 μmol kg⁻¹, i.e., salinity 35 diluted to 20, but almost no secondary precipitation at a DOC concentration of 325 μmol kg⁻¹,
361 i.e., about one and a half times higher than in the salinity 35. CaCO₃ precipitation was delayed by about two days when
362 doubling DOC concentration, and completely prevented at even higher levels (Figure 5) within the timeframe of the experiment
363 (1 week). Together, these data suggest that seawater DOC and Mg act in synergy when it comes to inhibiting CaCO₃
364 precipitation.

365 Another interesting finding was the new steady state reached after runaway CaCO₃ precipitation. In natural seawater
366 at a salinity of 36, the equilibrated Ω_A was estimated around 2.0, which is about 0.8 units lower than the starting conditions
367 (Figure 4). The decrease in Ω_A after runaway precipitation has important implications for OAE, as when CaCO₃ precipitates
368 in a runaway fashion, seawater can become more acidic than it was prior to mineral dissolution and less able to sequester
369 atmospheric CO₂ (Moras et al., 2022). While further work is required to understand these carbonate chemistry mechanisms at



370 lower salinities, we can note that after runaway precipitation in seawater at a salinity of 20, the final Ω_A was higher than the
371 starting one. Such a difference is likely due to the lower starting Ca^{2+} concentration at lower salinity.

372

373 **5. Conclusions**

374 One main objective of this research was to assess the dissolution of $\text{Mg}(\text{OH})_2$ in seawater at varying salinity, and
375 using different mineral grain sizes, and report on the subsequent CaCO_3 precipitation kinetics. The dissolution of $\text{Mg}(\text{OH})_2$ in
376 natural seawater occurred at a much faster rate when using grain sizes lower than $63\ \mu\text{m}$, due to the higher surface area in
377 contact with seawater. In contrast, bigger particles ($>63\ \mu\text{m}$) took about four times as long to fully dissolve. In all experiments,
378 CaCO_3 precipitation occurred in a runaway fashion, i.e. after a period of seeming stability, TA decreased rapidly before a new
379 steady state was reached at which TA reached concentrations far lower than prior to the $\text{Mg}(\text{OH})_2$ addition. A major finding
380 was that two processes occur during CaCO_3 precipitation in relation to grain size, one where the higher surface area of smaller
381 particles increases precipitation rates, while the second maintains a higher pH around larger particles due to a larger diffusive
382 boundary layer compared to smaller particles, which increases precipitation rates. Hence, there appears to be an optimum grain
383 size to minimise secondary CaCO_3 precipitation. The second objective of this research was to understand the role of salinity
384 on $\text{Mg}(\text{OH})_2$ dissolution and CaCO_3 precipitation kinetics. While no obvious changes in dissolution were observed, CaCO_3
385 precipitation differed, with a quicker precipitation observed at lower salinities. The decrease in Mg concentrations was
386 identified as the root cause, although in our experiments it was also linked to a lowered DOC concentration, an artefact of low
387 salinity seawater preparation by dilution with MilliQ. Nevertheless, this highlights the importance of DOC in modifying CaCO_3
388 precipitation kinetics and hence, TA stability.

389

390 **Data availability**

391 All data will be made available upon acceptance of the manuscript by *Biogeosciences*.

392

393 **Author contributions**

394 CAM and KGS designed the initial experiments with inputs from TC and LTB. CAM ran all the experiments and
395 with the help of KGS designed the follow-up experiments with MgCl_2 and DOC. The ICP-MS analyses were performed by
396 CAM and RJB, while CAM and KGS performed the SEM analyses. The first draft of the manuscript was written by CAM
397 with inputs from KGS, and all co-authors have helped writing and reviewing the manuscript for submission.

398



399 **Competing interests**

400 At least one of the (co-)authors is a member of the editorial board of *Biogeosciences*.

401

402 **Acknowledgments**

403 We would like to sincerely thank Atlas Materials for providing the magnesium hydroxide. We are also thankful to
404 Nick Ward for accommodating the use of the Scanning Electron Microscope, as well as Matheus Carvalho de Carvalho for the
405 dissolved organic carbon analyses.

406

407 **Financial support**

408 This research is part of the PhD project of Charly A. Moras that is funded by a Cat. 5 – SCU Grad School scholarship
409 from the Southern Cross University, Lismore, Australia. The ICP-MS analyses were made possible by Australian Research
410 Council grants to Renaud Joannes-Boyau and Kai G. Schulz (grant no. LE200100022) and to Renaud Joannes-Boyau (grant
411 no. LE120100201).

412



413 **References**

- 414 Carvalho, M. C., Eickhoff, W., and Drexler, M.: Open-source autosampler for elemental and isotopic analyses of solids,
415 *HardwareX*, 8, e00123, 10.1016/j.ohx.2020.e00123, 2020.
- 416 Chave, K. E. and Suess, E.: Calcium carbonate saturation in seawater: Effects of dissolved organic matter, *Limnology and*
417 *Oceanography*, 15, 633-637, 10.4319/lo.1970.15.4.0633, 1970.
- 418 Dickson, A. G., Sabine, C. L., and Christian, J. R.: Guide to best practices for ocean CO₂ measurements, PICES Special
419 Publication 3; IOCCP Report 8, Sidney, British Columbia, North Pacific Marine Science Organization, 191 pp.,
420 10.25607/OBP-1342, 2007.
- 421 Eisaman, M. D., Geilert, S., Renforth, P., Bastianini, L., Campbell, J., Dale, A. W., Foteinis, S., Grasse, P., Hawrot, O.,
422 Löscher, C. R., Rau, G. H., and Rønning, J.: Assessing the technical aspects of ocean-alkalinity-enhancement approaches,
423 *Guide to Best Practices in Ocean Alkalinity Enhancement Research*, 2-oae2023, 3, 10.5194/sp-2-oae2023-3-2023, 2023.
- 424 Friedlingstein, P., Jones, M. W., O'Sullivan, M., Andrew, R. M., Bakker, D. C. E., Hauck, J., Le Quéré, C., Peters, G. P.,
425 Peters, W., Pongratz, J., Sitch, S., Canadell, J. G., Ciais, P., Jackson, R. B., Alin, S. R., Anthoni, P., Bates, N. R., Becker, M.,
426 Bellouin, N., Bopp, L., Chau, T. T. T., Chevallier, F., Chini, L. P., Cronin, M., Currie, K. I., Decharme, B., Djutchouang, L.
427 M., Dou, X., Evans, W., Feely, R. A., Feng, L., Gasser, T., Gilfillan, D., Gkritzalis, T., Grassi, G., Gregor, L., Gruber, N.,
428 Gürses, Ö., Harris, I., Houghton, R. A., Hurtt, G. C., Iida, Y., Ilyina, T., Luijkx, I. T., Jain, A., Jones, S. D., Kato, E., Kennedy,
429 D., Klein Goldewijk, K., Knauer, J., Korsbakken, J. I., Körtzinger, A., Landschützer, P., Lauvset, S. K., Lefèvre, N., Lienert,
430 S., Liu, J., Marland, G., McGuire, P. C., Melton, J. R., Munro, D. R., Nabel, J. E. M. S., Nakaoka, S. I., Niwa, Y., Ono, T.,
431 Pierrot, D., Poulter, B., Rehder, G., Resplandy, L., Robertson, E., Rödenbeck, C., Rosan, T. M., Schwinger, J., Schwingshackl,
432 C., Séférian, R., Sutton, A. J., Sweeney, C., Tanhua, T., Tans, P. P., Tian, H., Tilbrook, B., Tubiello, F., van der Werf, G. R.,
433 Vuichard, N., Wada, C., Wanninkhof, R., Watson, A. J., Willis, D., Wiltshire, A. J., Yuan, W., Yue, C., Yue, X., Zaehle, S.,
434 and Zeng, J.: Global carbon budget 2021, *Earth System Science Data*, 14, 1917-2005, 10.5194/essd-14-1917-2022, 2022.
- 435 Fuhr, M., Geilert, S., Schmidt, M., Liebetrau, V., Vogt, C., Ledwig, B., and Wallmann, K.: Kinetics of Olivine Weathering in
436 Seawater: An Experimental Study, *Frontiers in Climate*, 4, 10.3389/fclim.2022.831587, 2022.
- 437 Gafar, N. A. and Schulz, K. G.: A three-dimensional niche comparison of *Emiliania huxleyi* and *Gephyrocapsa oceanica*:
438 reconciling observations with projections, *Biogeosciences*, 15, 3541-3560, 10.5194/bg-15-3541-2018, 2018.
- 439 GESAMP: High level review of a wide range of proposed marine geoengineering techniques. (Boyd, P.W. and Vivian, C.M.G.,
440 eds.). (IMO/FAO/UNESCO-IOC/UNIDO/WMO/IAEA/UN/UN Environment/UNDP/ISA Joint Group of Experts on the
441 Scientific Aspects of Marine Environmental Protection). Rep. Stud. GESAMP No. 98, 144 p.1020-4873, 2019.
- 442 Gore, S., Renforth, P., and Perkins, R.: The potential environmental response to increasing ocean alkalinity for negative
443 emissions, *Mitigation and Adaptation Strategies for Global Change*, 24, 1191-1211, 10.1007/s11027-018-9830-z, 2019.



- 444 Hartmann, J., Suitner, N., Lim, C., Schneider, J., Marín-Samper, L., Aristegui, J., Renforth, P., Taucher, J., and Riebesell, U.:
445 Stability of alkalinity in ocean alkalinity enhancement (OAE) approaches – consequences for durability of CO₂ storage,
446 *Biogeosciences*, 20, 781-802, 10.5194/bg-20-781-2023, 2023.
- 447 Hartmann, J., West, A. J., Renforth, P., Köhler, P., De La Rocha, C. L., Wolf-Gladrow, D. A., Dürr, H. H., and Scheffran, J.:
448 Enhanced chemical weathering as a geoengineering strategy to reduce atmospheric carbon dioxide, supply nutrients, and
449 mitigate ocean acidification, *Reviews of Geophysics*, 51, 113-149, 10.1002/rog.20004, 2013.
- 450 Hoegh-Guldberg, O., Jacob, D., Taylor, M., Guillén Bolaños, T., Bindi, M., Brown, S., Camilloni, I. A., Diedhiou, A., Djalante,
451 R., Ebi, K., Engelbrecht, F., Guiot, J., Hijikata, Y., Mehrotra, S., Hope, C. W., Payne, A. J., Pörtner, H.-O., Seneviratne, S. I.,
452 Thomas, A., Warren, R., and Zhou, G.: The human imperative of stabilizing global climate change at 1.5 °C, *Science*, 365,
453 eaaw6974, 10.1126/science.aaw6974, 2019.
- 454 IPCC: Summary for Policymakers. In: *Climate Change 2021: The Physical Science Basis. Contribution of Working Group I*
455 *to the Sixth Assessment Report of the Intergovernmental Panel on Climate Change* [Masson-Delmotte, V., P. Zhai, A. Pirani,
456 S.L. Connors, C. Péan, S. Berger, N. Caud, Y. Chen, L. Goldfarb, M.I. Gomis, M. Huang, K. Leitzell, E. Lonnoy, J.B.R.
457 Matthews, T.K. Maycock, T. Waterfield, O. Yelekçi, R. Yu, and B. Zhou (eds.)], Cambridge University Press, Cambridge,
458 United Kingdom and New York, NY, USA, pp. 3-32, 10.1017/9781009157896.001, 2021.
- 459 Kheshgi, H. S.: Sequestering atmospheric carbon dioxide by increasing ocean alkalinity, *Energy*, 20, 915-922, 10.1016/0360-
460 5442(95)00035-F, 1995.
- 461 Lewis, E. L. and Perkin, R. G.: The practical salinity scale 1978: conversion of existing data, *Deep Sea Research Part A.*
462 *Oceanographic Research Papers*, 28, 307-328, 10.1016/0198-0149(81)90002-9, 1981.
- 463 Lioliou, M. G., Paraskeva, C. A., Koutsoukos, P. G., and Payatakes, A. C.: Heterogeneous nucleation and growth of calcium
464 carbonate on calcite and quartz, *Journal of Colloid and Interface Science*, 308, 421-428, 10.1016/j.jcis.2006.12.045, 2007.
- 465 Lüthi, D., Le Floch, M., Bereiter, B., Blunier, T., Barnola, J.-M., Siegenthaler, U., Raynaud, D., Jouzel, J., Fischer, H.,
466 Kawamura, K., and Stocker, T. F.: High-resolution carbon dioxide concentration record 650,000–800,000 years before present,
467 *Nature*, 453, 379-382, 10.1038/nature06949, 2008.
- 468 Marion, G. M., Millero, F. J., and Feistel, R.: Precipitation of solid phase calcium carbonates and their effect on application of
469 seawater SA - T - P models, *Ocean Science*, 5, 285-291, 10.5194/os-5-285-2009, 2009.
- 470 Millero, F., Huang, F., Zhu, X., Liu, X., and Zhang, J.-Z.: Adsorption and desorption of phosphate on calcite and aragonite in
471 seawater, *Aquatic Geochemistry*, 7, 33-56, 10.1023/A:1011344117092, 2001.
- 472 Monnin, E., Indermühle, A., Dällenbach, A., Flückiger, J., Stauffer, B., Stocker, T. F., Raynaud, D., and Barnola, J. M.:
473 Atmospheric CO₂ concentrations over the last glacial termination, *Science*, 291, 112-114, 10.1126/science.291.5501.112,
474 2001.



- 475 Montserrat, F., Renforth, P., Hartmann, J., Leermakers, M., Knops, P., and Meysman, F. J. R.: Olivine dissolution in seawater:
476 Implications for CO₂ sequestration through enhanced weathering in coastal environments, *Environmental Science &*
477 *Technology*, 51, 3960-3972, 10.1021/acs.est.6b05942, 2017.
- 478 Moras, C. A., Bach, L. T., Cyronak, T., Joannes-Boyau, R., and Schulz, K. G.: Ocean alkalinity enhancement – avoiding
479 runaway CaCO₃ precipitation during quick and hydrated lime dissolution, *Biogeosciences*, 19, 3537-3557, 10.5194/bg-19-
480 3537-2022, 2022.
- 481 Moras, C. A., Bach, L. T., Cyronak, T., Joannes-Boyau, R., and Schulz, K. G.: Preparation and quality control of in-house
482 reference materials for marine dissolved inorganic carbon and total alkalinity measurements, *Limnology and Oceanography:*
483 *Methods*, 10.1002/lom3.10570, 2023.
- 484 Morse, J. W., Arvidson, R. S., and Lüttge, A.: Calcium carbonate formation and dissolution, *Chemical Reviews*, 107, 342-
485 381, 10.1021/cr050358j, 2007.
- 486 Pan, Y., Li, Y., Ma, Q., He, H., Wang, S., Sun, Z., Cai, W.-J., Dong, B., Di, Y., Fu, W., and Chen, C.-T. A.: The role of Mg²⁺
487 in inhibiting CaCO₃ precipitation from seawater, *Marine Chemistry*, 237, 104036, 10.1016/j.marchem.2021.104036, 2021.
- 488 Pytkowicz, R. M.: Rates of inorganic calcium carbonate nucleation, *The Journal of Geology*, 73, 196-199, 10.1086/627056,
489 1965.
- 490 Sharp, J., Pierrot, D., Humphreys, M., Epitalon, J., Orr, J., Lewis, E., and Wallace, D.: CO2SYSv3 for MATLAB, Zenodo
491 [code], 10, 10.5281/zenodo.3950562, 2021.
- 492 Siegenthaler, U., Stocker, T. F., Monnin, E., Lüthi, D., Schwander, J., Stauffer, B., Raynaud, D., Barnola, J. M., Fischer, H.,
493 Masson-Delmotte, V., and Jouzel, J.: Stable carbon cycle-climate relationship during the Late Pleistocene, *Science*, 310, 1313-
494 1317, 10.1126/science.1120130, 2005.
- 495 Zeebe, R. E. and Wolf-Gladrow, D.: CO₂ in seawater: equilibrium, kinetics, isotopes, 65, Gulf Professional Publishing, 360
496 pp.2001.
- 497 Zhong, S. and Mucci, A.: Calcite and aragonite precipitation from seawater solutions of various salinities: Precipitation rates
498 and overgrowth compositions, *Chemical Geology*, 78, 283-299, 10.1016/0009-2541(89)90064-8, 1989.